

Freeze-out prevention of iso-pentane in mixtures with light hydrocarbons at cryogenic conditions applicable for safe mixed refrigerants

Mirhadi S. Sadaghiani¹, Arman Siahvashi¹, Bruce W. E. Norris¹, Saif Al Ghafri¹, Arash

Arami-Niya², Eric F. May^{*1}

¹ Fluid Science & Resources Division, Department of Chemical Engineering, The University of Western Australia, 35 Stirling Hwy, Crawley 6009, Australia

² Discipline of Chemical Engineering, Western Australian School of Mines: Minerals, Energy and Chemical Engineering, Curtin University, GPO Box U1987, Perth, WA 6845, Australia

Abstract

A visual, high-pressure equilibrium cell was used to investigate freezing and melting points for iso-pentane and its mixtures with other hydrocarbons as a potential component for LNG plants' mixed refrigerants. The freezing and melting temperatures were measured for highly pure iso-pentane, industrial-grade pure iso-pentane, and methane + iso-pentane binary systems, at temperatures down to 87.5 K and pressures up to 13 MPa. A thermodynamic model embedded in the ThermoFAST software package was tuned to the pure iso-pentane experimental melting points to address the trending deviation of predicted melting temperatures by the pressure. This investigation showed that the melting and freezing points of highly purified and industrial-grade iso-pentane were less sensitive to pressure, increasing with an average rate of 0.2 K/MPa by the pressure. The experimental melting and freezing points for binary mixtures were measured as a benchmark to assess the worst-case scenario for designing the mixed refrigerant

* E-mail addresses: Eric.May@uwa.edu.au

mixtures containing heavy hydrocarbons like iso-pentane. The methane richer mixtures of the binary system had melting temperatures less than 100 K, while for iso-pentane rich blends, the melting temperature was limited between (100-105) K.

Keywords: Solubility, Mixed Refrigerant, iso-pentane, Melting Temperature, Freezing Temperature

1. Introduction

The global decarbonisation process attracted considerable demand for liquefied natural gas (LNG) as a clean energy source [1] and improved its potential to overtake coal in overall demand by 2035 [2]. A large amount of power required for treatment, compression and refrigeration of natural gas makes the liquefaction the most energy-intensive part of the LNG supply chain [3]. Before the liquefaction step, impurities like heavy hydrocarbons, water, and acid gasses need to be removed from the natural gas [4–6]. The presence of heavy hydrocarbons, including heavier components than butane (C5+) in (LNG) production streams at trace concentration, can pose significant challenges of blockage and plant shutdown [7–9]. Thermodynamic models are crucial to identify and predict those heavy hydrocarbons' concentration limits. These models are anchored to reliable and relevant solid–fluid equilibrium (SFE) data; unfortunately, such data are sparse. Robust and reliable data and models are required to help make informed decisions for either the design or the operation of LNG facilities. These models determine acceptable limits of solid-forming compounds in the cryogenic fluids to ensure a negligible risk of freeze-out [10].

The freeze-out risk associated with such heavy hydrocarbons is also essential in refrigeration units of the LNG plants. While a cascade of independent single component refrigeration loops remains the most popular option, mixed refrigerant (MR) systems offer an attractive alternative because of their efficient heat transfer and high energy efficiency [11]. Using heavier components like iso-butane and iso-pentane in mixed refrigerant can exploit the latent heat

transfer and reduce the refrigerant circulation rate, resulting in smaller equipment size and higher liquefaction efficiency [12–16]. In their most advanced form, these mixed refrigerant systems use a single fluid process stream flashed through several stages of the liquefaction process, delivering heavy and light fractions with tuneable boiling points [17]. This dynamic control of the cooling curve inside the primary heat exchangers improves energy efficiency and decreases the LNG production chain's unit cost. As these mixed refrigerant systems contain multiple components, there is a possibility of heavy-species freeze-out, where the exact freezing curve is not as easily determined as in the case of pure component systems.

Several studies reported the melting point for iso-pentane; Acree [18] measured thermodynamic properties of organic compounds and noted a melting temperature of 113.25 K for iso-pentane. Preston et al. [19] studied solubility of iso-pentane in liquid methane and measured a fusion temperature of 113.2 K for iso-pentane. Parks and Huffman [20] measured a melting temperature of 112.65 K for iso-pentane, while Schumann et al. [21] reported 113.39 K for iso-pentane melting temperature. No data were reported for melting temperature of pure iso-pentane and its mixtures with lighter hydrocarbons at elevated pressures.

This study extends the experimental data body for pure iso-pentane melting and freezing points to LNG facilities' process conditions by using the specialised CryoSolid apparatus developed at the University of Western Australia (UWA). Therefore, a total of 20 freezing and melting points for pure iso-pentane, and 8 freezing and melting points for binary mixtures of methane + iso-pentane were measured. The experimental results were compared with the predictions of ThermoFAST; a software package developed at UWA, which uses Peng-Robinson equation of state (PR-EOS) model together with an equation for predicting the solid's fugacity to estimate melting temperatures. Ultimately, this work seeks to decrease the uncertainty associated with determining the freeze-out possibility for mixed refrigerants containing iso-pentane as their heavy component.

2. Material and Methods

A visual method of solid identification similar to the one described in our previous publications used in this study [6,8]. The measurement setup includes an injection system, a high-pressure sapphire cell located inside an environmental cooling chamber and a data acquisition system.

2.1 Material

Details of iso-pentane and methane components (their sources and purities) used in this work to prepare the binary mixtures were summarised in Table 1. The liquid iso-pentane was used without further purification. However, upon loading the solute before starting the measurement, the liquid was degassed by evacuating any dissolved gas present using a vacuum pump (Vacuubrand MZ2C).

Table 1: Details of the chemicals used in this work with the corresponding grade, specified purity, and specified dominant impurities.

Chemical Name	Supplier	Grade and Purity Mole Fraction	Impurities	CAS Number
Iso-pentane (2-Methylbutane)	Merck (Sigma Aldrich)	Anhydrous ≥ 0.995	<0.02% Water <0.0003% Evap. Residue	78-78-4
Iso-pentane (2-Methylbutane) – industrial grade	CoreGas Australia	Pressurised liquid ≥ 0.99	<1.00 % benzene < 5 ppm water < 0.5 ppm sulphur	78-78-4
Methane	CoreGas Australia	Compressed Gas ≥ 0.999995	-	74-82-8

2.2 CryoSolid Apparatus Overview

Figure 1 illustrates the schematic diagram of the measurement system, called CryoSolid setup. A transparent equilibrium cell capable of operating at pressures up to 31 MPa was connected to a mixture preparation unit. The environmental cooling chamber (M170J-13100) with a Thermal Solution Series controller (KTS6310AB), hosted the equilibrium cell, had an operational temperature range of (87 to 473) K, which a high-pressure liquid nitrogen (LN₂)

Dewar supplied the required LN₂ to the chamber. Figure 2 shows the transparent high-pressure equilibrium cell as the central component of the CryoSolid setup that consisted of a high precision sapphire tube with 70 mL volume. The cell was fitted with a copper cold finger, used when the compound's concentration under study is not in excess. In this work, only the bulk fluid temperature was adjusted to determine the freezing and melting measurements.

The maximum cooling or heating rate applied to the CryoSolid apparatus was limited to 1 K/min to minimise the risk of thermal shock or damage to the system, especially to the sapphire tube. Fast response 100 Ω platinum resistance thermometers (PRT NR-14, Netsushin) was employed to measure the temperature of the main body, top flange and copper tip. Only the copper tip temperature was reported in this study, which the temperature sensor was bored into the copper post through a blind well. All PRTs were calibrated by a reference standard PRT sensor (ASL-WIKA) with a standard uncertainty of 0.02 K over a temperature range of 100-273 K. A quartz-crystal pressure transducer (Digiquartz, Paroscientific) with a full scale of 30 MPa was employed to measure the pressure of the mixture inside the cell. A stepper motor (Arun Micro-electronics D42.2) drove the stirrer bar by coupling to a custom-made magnetic shaft.

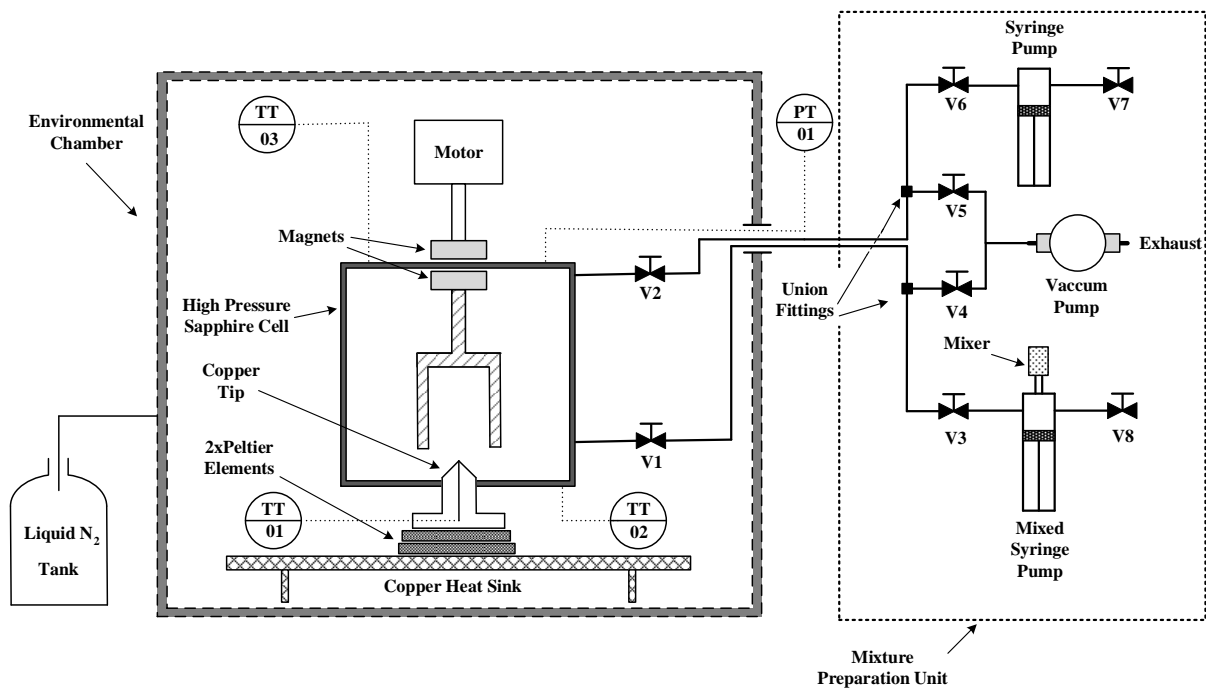


Figure 1: Schematic Diagram of the CryoSolids apparatus.

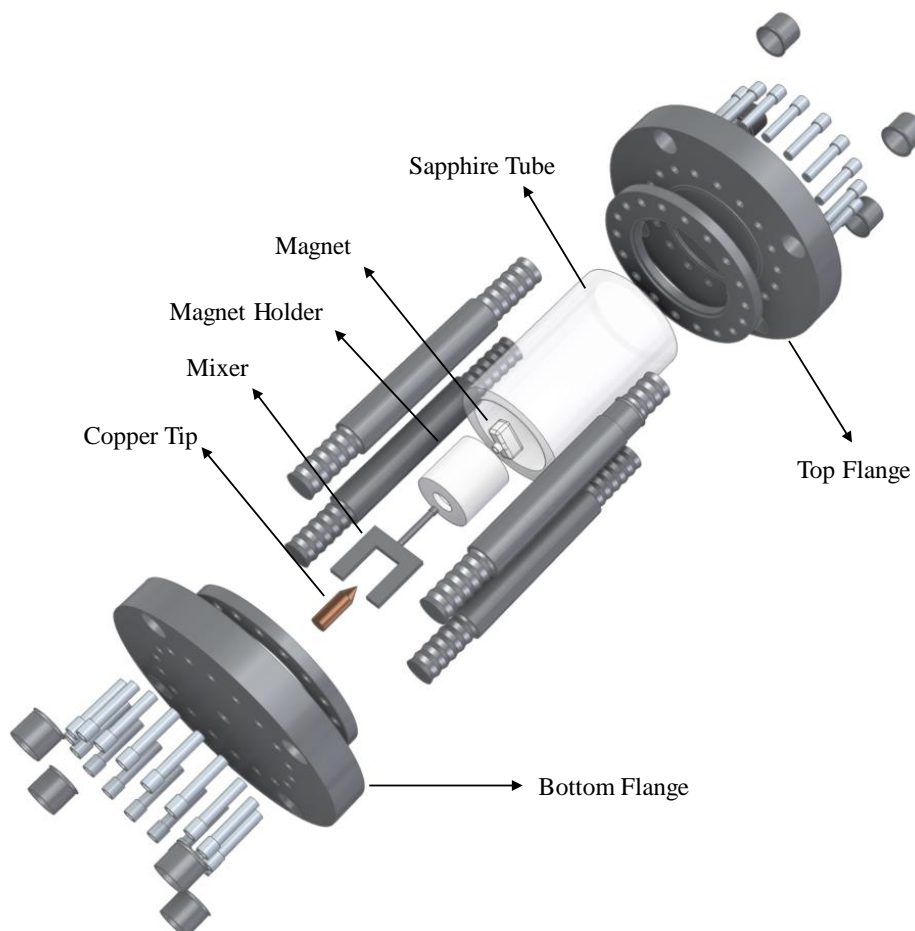


Figure 2: The visual cell assembly's exploded view.

2.3 Mixture Preparation Unit

The mixture preparation unit included two syringe pumps: (1) a high-pressure syringe pump (Teledyne ISCO 500 HP) with an external stirrer (Buchiglassuster Cyclone-075) and volume of 500 mL; (2) a high precision syringe pump (Teledyne ISCO 260D) with 260 mL volume. The mixture preparation process started with injecting the heaviest component of the mixture and proceeded to lighter components. ISCO 260D syringe pump was used to inject the predetermined volumes of components at constant pressure into the stirred syringe pump to prepare the target mixtures. The syringe pumps were capable of injection at flow rates ranging from 0.01 to 107 ml/min under controlled pressures ranging from 0.07 to 52 MPa. Then, the final mixture left under continuous stirring during the measurement inside the syringe pump to ensure the synthesised mixture's homogeneity.

2.3 Measurement Procedures

Before starting the measurements, the equilibrium cell was pre-cleaned with appropriate solvents and evacuated using a vacuum pump (Varian SH-110). The desired amount of the binary mixture or pure iso-pentane was injected into the cell by the stirred syringe pump at ambient temperature (measured by an independent 100 Ω PRT) to achieve the target pressure in the cell. The internal temperature of the environmental cooling chamber was declined through supplying LN₂ from the high-pressure Dewar at a controlled rate of 1 K/min. This cooling rate decreased the cell content's temperature at a rate below 0.8 K/min while the mixture was under continuous stirring. Ultimately, the cooling chamber and the equilibrium cell temperatures were stabilised by PID control algorithms at the desired set-points. The temperature in the cell, measured by sensor TT01 and TT02, was then reduced in steps by adjusting the chamber cooling rate until the first solid crystals formed. This point was noted as

the freezing point (T_f). Following the compound freeze-out, the temperature was increased at a rate between 0.1 and 0.2 K/min to the point where all last solid crystal melted (T_m).

2.4 Solid Formation and Dissociation Process

The physical state of a substance dictates its thermophysical properties; generally, chemical properties, bond energies and molecular shape of a substance are determined by covalent bonds (chemical bonds), while boiling and melting points, density, and solubility depend upon the intermolecular forces between the substance's molecules [22]. Molecules of alkanes are bonded to each other by weak van der Waals' forces; which the strength of these intermolecular forces increases by the molecular mass of the alkane. Figure 3 shows the freezing process of iso-pentane inside the visual cell along with the molecular structure of each phase. In liquid iso-pentane, the attractive intermolecular forces can keep the molecules close together, while upon freezing, the strength of the van der Waals' forces increases and keep the molecules locked in positions relative to their neighbours. Figure 4 indicates the solid nucleation and dissociation processes of iso-pentane + methane binary mixture (41.48:58.52 mole%). A supercooling of 5.6 K was required to induce the nucleation process in this binary mixture. Each experimental point repeated 3 times to ensure the reliability of the measured freezing and melting temperatures. Panasonic high-definition (HD) camcorder (HCV 180) was employed to capture and record the solid freezing and melting points. In addition to the chamber's build-in illumination, extra lights were used to achieve sufficient background light levels for high-quality image capture by the camera.

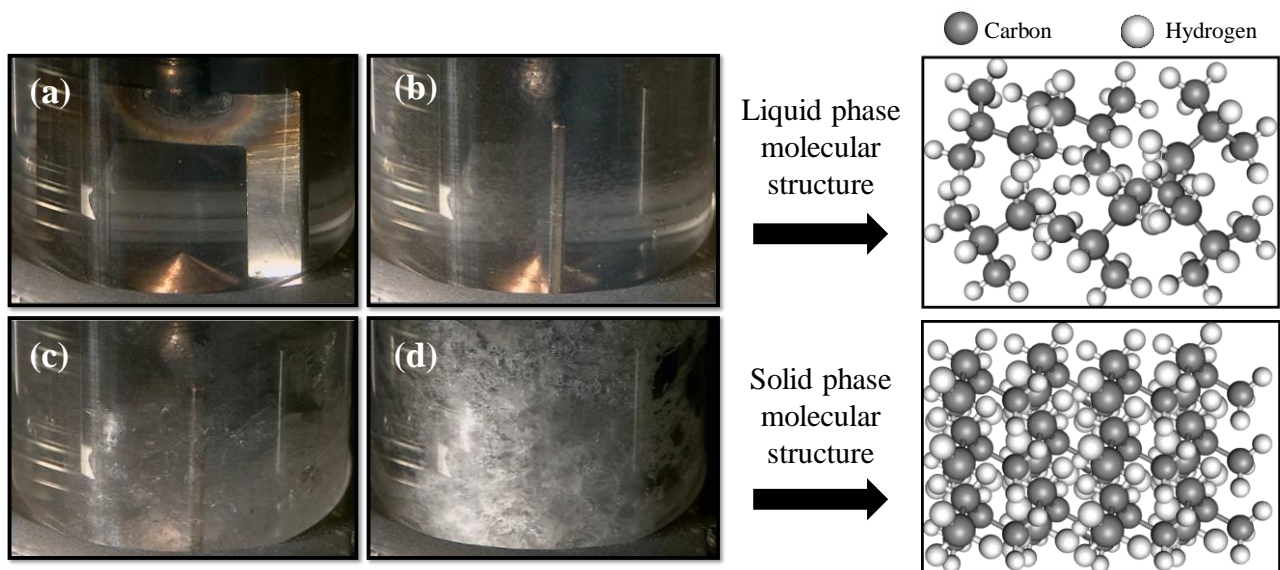


Figure 3: Freezing process of pure iso-pentane: (a) subcooled iso-pentane liquid ($p=13$ MPa, $T=108.8$ K); (b) and (c) solid-liquid equilibrium (SLE) mixtures of iso-pentane ($p =13$ MPa, $T = 108.3$ K); (d) solid iso-pentane ($p =13$ MPa, $T = 108.3$ K).

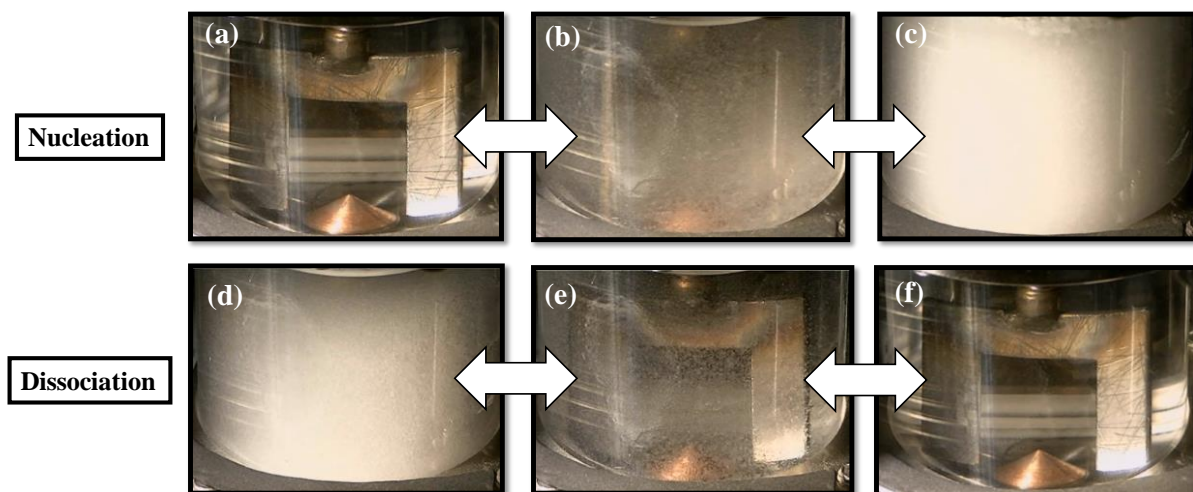


Figure 4: Solid nucleation and dissociation processes of iso-pentane + methane binary mixture (41.48:58.52 mole%) at 0.03 MPa: (a) $T = 94.1$ K (supercooled liquid); (b) $T = 93.9$ K (solid-liquid equilibrium); (c) $T = 93.5$ K; (d) $T = 98.8$ K; (e) $T = 99.3$ K; (f) $T = 99.5$ K (no solids).

3. Model

3.1 Experimental Uncertainty

Contributions to the combined standard uncertainty in the measured melting and freezing temperatures (T_m and T_f) were considered according to the outlines of the “Guide to the Expression of Uncertainty in Measurement” [23], developed by NIST:

$$u^2(x_i) = \sum_{j=1}^n \left[\left(\frac{\partial x_i}{\partial z_j} \right)^2 u^2(z_j) \right] \quad (1)$$

where $z_{j=1,2,\dots,n}$ denote the n independent variables that x_i depends upon, each associated with variance of $u^2(z_j)$. The experimental uncertainty assessment for the temperature and pressure measurements were detailed in our previous works [8,24,25]. To sum up, the standard uncertainty in the measured dissociation temperature was estimated by considering the standard deviation of the repeated measurements (in range of ± 0.3 K) along with the standard uncertainty of the PRT sensors (estimated to 0.05 K). The standard uncertainty in pressure measurements was estimated to be 0.02 MPa, taking into account temperature and pressure fluctuations. The standard uncertainty in mole fractions of the prepared refrigerant mixtures was estimated by considering the cumulative effects of uncertainty in the injected volume, pressure and temperature of the syringe pump along with the uncertainty of the density of the equation of state embedded in the NIST software package REFPROP 10 [26].

3.2 Freeze-out Model

This section describes the utilised thermodynamic model for the freeze-out model and solid-liquid-equilibrium (SLE) calculations as implemented in ThermoFAST software package; Peng-Robinson cubic equation of state (PR EOS) is used to predict the SLE conditions for single or multi-component solutions [27,28]:

$$p = \frac{RT}{v - b_m} - \frac{a_m}{[v + (1 + \sqrt{2})b_m][v + (1 - \sqrt{2})b_m]} \quad (2)$$

here, p , T , R , and v stand for the pressure, temperature, universal molar gas constant, and molar volume. The a_m and b_m parameters represent the mixing parameters, which can be calculated through the van der Waals mixing rules:

$$a_m = \sum_i \sum_j x_i x_j [(1 - k_{ij}) \sqrt{a_i a_j}] \quad (3)$$

$$b_m = \sum_i x_i b_i$$

where x_i , x_j , and k_{ij} are the mole fraction of component i and j , and the binary interaction parameter (BIP); the last parameter is a tuning constant that can improve the consistency of the model's prediction to the experimental values. Parameters a_i and b_i , standing for temperature-dependent energy and co-volume parameters, can be determined for a single-component fluid by:

$$a_i = 0.457235 \frac{(RT_{c,i})^2}{p_{c,i}} \alpha_i$$

$$b = 0.077796 \frac{RT_{c,i}}{p_{c,i}} \quad (4)$$

$$\alpha_i = [1 + m_i(1 - \sqrt{(T/T_{c,i})})]^2$$

$$m_i = 0.37464 + 1.5226\omega_i - 0.26992\omega_i^2$$

where ω_i , $T_{c,i}$ and $p_{c,i}$ are the acentric factor, critical temperature, and critical pressure of component i , respectively. The partial fugacities for the individual component i that forms the solid phase should be equal for both phases as follows:

$$f_i^{pure,s}(p, T) = f_i^{mix,l}(p, T, x_i^{mix,l}) \quad (5)$$

In the present study, the solid phase is considered as a pure component and the liquid phase as either a single component, binary or multi-component mixture. The solubility of component i could be obtained by a thermodynamic model endorsed by Prausnitz et al. [29] as:

$$\frac{f_i^s}{f_i^l} = x_i \gamma_i = \exp \left[\left(\frac{T_i^{fus} \Delta C_{P,i}^{fus} - \Delta H_i^{fus}}{R} \right) \left(\frac{1}{T} - \frac{1}{T_i^{fus}} \right) + \frac{\Delta C_{P,i}^{fus}}{R} \ln \frac{T}{T_i^{fus}} - \frac{(P - P_0) \Delta v_i^{fus}}{RT} \right] \quad (6)$$

here, f_i^s , f_i^l stand for the fugacity of the pure solid and liquid phases of component i , while T_i^{fus} , P_0 and γ_i represent the normal melting point temperature, the atmospheric pressure and

the liquid phase activity coefficient of component i . $\Delta c_{p,i}^{fus}$, ΔH_i^{fus} and Δv_i^{fus} are the molar heat capacity, molar enthalpy and molar volume changes of fusion at the melting point of component i , respectively. Table 2 lists the experimental and calculated value for iso-pentane fusion properties in the literature.

Table 2: Pure iso-pentane fusion parameters used in ThermoFAST freeze-out model

Parameter	T_{iC5}^{fus} / K	$\Delta H_{iC5}^{fus} / \text{J.mol}^{-1}$	$\Delta c_{p,iC5}^{fus} / \text{J} \cdot (\text{mol.K})^{-1}$	$\Delta v_{iC5}^{fus*} / \text{m}^3 \cdot \text{mol}^{-1}$
iso-pentane	113.2	5147	32.194	1.34E-5
Ref.	[19]	[21,30]	[21]	[31,32]

* This particular property is calculated using the difference in density of the solid and the liquid at the melting point temperature based on the mentioned references.

The molar volume change on fusion was optimized based on the experimental data of pure iso-pentane by using Generalised Reduced Gradient (GRG) algorithm encoded within the solver tool of Microsoft Excel software [33].

4. Results and Discussion

4.1 Pure and industrial iso-pentane

Freezing and melting temperatures for the pure and industrial-grade iso-pentane samples were measured at isobaric pressures between (0.25 and 13.04) MPa. After charging the cell with liquid iso-pentane to a target starting pressure, the sample was stirred continuously at 300 RPM to assure the mixture remained in a thermally homogenous state as the cell was cooled. A total of ten data points for each type of iso-pentane were obtained for the freezing and melting temperatures as a function of pressure, presented in Table 3. Figure 5 (a) illustrates the measured freezing and melting temperatures at different pressures. The average cooling and heating rates to obtain the freezing and melting temperatures were $\beta_{f,ave} = 0.5 \text{ K/min}$ and $\beta_{m,ave} = 0.1 \text{ K/min}$, respectively. The average undercooling ($T_f - T_m$) for the entire data set was down

to 8 K to form a seed solid or nucleus around which a solid structure can form. Absence of any such nuclei can lead the supercooled liquid phase stable down to the temperature at which homogeneous nucleation undertakes. Opposite to freezing point, solids almost always melt at the same temperature for a given pressure.

These results show that although a linear relationship exists between the melting (and freezing) temperatures and pressures, the freezing and melting temperatures are relatively less sensitive to pressure because of liquids' incompressibility. The rate at which the freezing and melting temperature increased with pressure was approximately 0.28 K/MPa and 0.13 K/MPa, respectively. Also, by adding impurities to iso-pentane, the solids were formed at higher temperatures than the pure iso-pentane and melted at lower temperatures.

The reported triple point in the literature varies between 112.65 K and 113.39 K [19,21,34,35]. According to Schumann et al. [21], the triple point of iso-pentane is 113.39 (± 0.05 K). Extrapolating our data from the lowest pressure measured (0.27 MPa) results in a triple point value of 113.41 K. The 0.02 K difference is well within our experimental uncertainty of 0.3 K.

Table 3: Measured freezing and melting temperature data for pure and industrial-grade iso-pentane.

Pure iso-pentane				Industrial iso-pentane			
p_f / MPa	T_f / K	p_m / MPa	T_m / K	p_f / MPa	T_f / K	p_m / MPa	T_m / K
0.25	104.55	0.27	113.45	0.20	106.1	0.21	112.9
1.88	105.20	1.89	113.64	2.05	106.3	2.07	113.3
5.05	106.12	5.06	114.04	4.35	106.6	4.37	113.5
7.04	106.72	7.06	114.33	7.06	107.1	7.07	113.9
13.04	108.32	13.06	115.17	13.05	109.1	13.06	114.6

* The overall uncertainties in the temperature and pressure measurements were 0.3 K and 0.02 MPa, respectively.

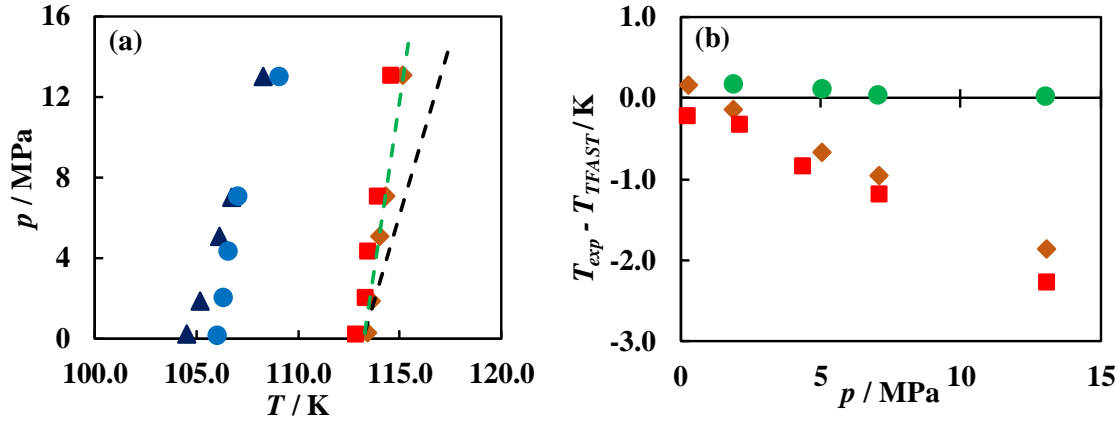


Figure 5: (a) Phase diagram showing the freezing and melting temperatures measured for pure and industrial-grade iso-pentane: \blacktriangle experimental freezing temperature (pure iso-pentane), \bullet experimental freezing temperature (industrial iso-pentane), \blacklozenge experimental melting temperature (pure iso-pentane), \blacksquare experimental melting temperature (industrial iso-pentane), --- melting temperature predicted by default ThermoFAST (pure iso-pentane), and --- melting temperature predicted by optimised ThermoFAST (pure iso-pentane); (b) deviations of the measured melting temperatures, T_{exp} , from those calculated by ThermoFAST software package, T_{calc} , as a function of pressure, p : \blacklozenge pure iso-pentane (default Δv_{iC5}^{fus}), \bullet pure iso-pentane (optimised Δv_{iC5}^{fus}), and \blacksquare industrial iso-pentane (default Δv_{iC5}^{fus}).

The measured melting temperature data were also compared with the predictions of ThermoFAST. Figure 5 (b) shows the deviation of the experimental data from the ones calculated using ThermoFAST model with fusion constants listed in Table 2. This graph shows that ThermoFAST systematically deviates from the experimental melting temperature data with average root mean square (RMS) values of 0.98 K and 1.22 K for pure and industrial iso-pentane, respectively. Such deviations were expected as no literature data exist on iso-pentane melting temperature as a function of pressure. A possible cause for this linear deviation could be the inaccurate estimation of the fusion molar volume variation for pure iso-pentane in the freeze-out model ($\Delta v_{iC5}^{fus} = 13.4E-6 \text{ m}^3 \cdot \text{mol}^{-1}$). An optimised value of ($\Delta v_{iC5}^{fus} = 6.94E-6 \text{ m}^3 \cdot \text{mol}^{-1}$) was calculated for the fusion molar volume variation of iso-pentane by tuning the freeze-out model according to the experimental melting points. This value is close to the reported value of ($\Delta v_{iC5}^{fus} = 7.3E-6 \text{ m}^3 \cdot \text{mol}^{-1}$) by Wurflinger and Kreutzenbeck [36]. The optimisation enabled ThermoFAST to represent the experimental melting points with an improved average RMS of 0.1 K for the pure iso-pentane.

4.2 iso-pentane + methane binary mixtures

No experimental data are available in the literature on solid-liquid-equilibrium of methane + iso-pentane binary mixtures. We attempted to measure the melting and freezing temperatures of this binary at different compositions and pressures. Table 4 presents the measured freezing and melting temperatures, pressures and overall composition of methane + iso-pentane binary mixtures. Figure 6 (a) shows the freezing and melting temperatures for the binary mixtures of methane + iso-pentane at different mole fractions of the latter component and pressure levels up to 10 MPa. The melting temperature of methane + iso-pentane binary mixture increases from 98.24 K to 105.45 K by increasing the iso-pentane mole fraction from 0.1988 to 0.5713.

Table 4: Measured freezing and melting temperature data for binary mixtures of methane + iso-pentane.

x_{iC5}	u_{xiC5}	p_f / MPa	T_f / K	p_m / MPa	T_m / K
0.1988	0.0050	10.05	93.28	10.07	98.24
0.2426	0.0050	7.55	92.76	7.57	98.52
0.4148	0.0050	0.02	93.71	0.04	100.07
0.5713	0.0023	0.03	95.15	0.06	105.45

* The overall uncertainties in the temperature and pressure were 0.3 K, 0.02 MPa and, respectively.

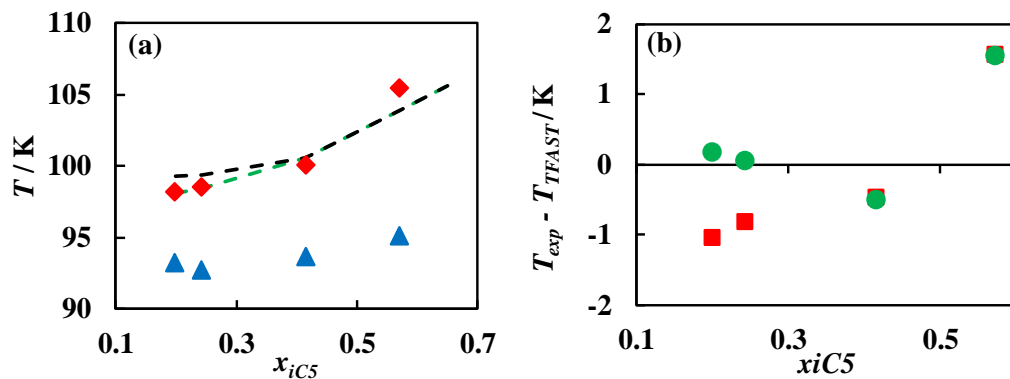


Figure 6: (a) The freezing and melting temperatures of methane-iso-pentane binary mixtures in terms of iso-pentane mole fraction: --- melting temperature predicted by default ThermoFAST, --- melting temperature predicted by optimised ThermoFAST ♦ experimental melting temperature and ▲ experimental freezing temperature; (b) deviations of the experimental melting temperatures, T_{exp} , from

those calculated by the ThermoFAST software package, T_{calc} , as a function iso-pentane mole fraction:

■ default Δv_{iC5}^{fus} and ● optimised Δv_{iC5}^{fus} .

This set of experimental data enable more accurate modelling of the relevant LNG / Mixed Refrigerant multi-component mixtures' properties because they allow confirming the predictions of the solubility of a heavy compound in a solvent mixture. The experimental data were used to double-check Peng-Robinson EOS (embedded in ThermoFAST) predictions for iso-pentane solubility in methane with the default and optimised fusion molar volume variation of pure iso-pentane. The default fusion molar volume variation results in an RMS deviation of 1 K with the experimental data, while the optimized value decreases the RMS deviation to 0.8 K. Figure 6 (b) illustrates the deviation of the experimental melting points from the predicted values by the default and optimized freeze-out models of ThermoFAST. The optimised freeze-out model represents methane rich mixtures (the first two points) accurately, with (0.2 and 0.1) K deviations; where the cell's pressure was at 10 and 7.5 MPa, respectively. However, the optimised model predicted iso-pentane richer mixtures with higher deviations of -0.5 and 1.5 K because the equilibrium pressure was insignificant at these points. While further experiments are needed to tune the model for the richer iso-pentane mixtures, those mixtures are out of the scope of the current research study.

5. Conclusions

The CryoSolids apparatus was deployed to determine the freezing and melting temperatures of six mixtures of interest experimentally: i) pure iso-pentane; ii) industrial-grade pure iso-pentane; and iii) binary mixtures of iso-pentane + methane at temperatures down to 87.5 K and pressures up to 13 MPa.

ThermoFAST with default freeze-out model constants described the melting temperature data measured for pure and industrial iso-pentane within RMS deviations of 0.98 and 1.22 K, respectively. The RMS deviation for pure iso-pentane decreased to 0.2 K by optimising the iso-pentane fusion molar volume variation based on the experimental points. Also, the industrial-

grade iso-pentane melted at slightly lower temperatures than pure iso-pentane because of the impurities (such as nC5, nC4, etc.), decreasing iso-pentane melting temperature. The measurements showed that the melting and freezing points of the liquid industrial grade and pure iso-pentane were less sensitive to pressure due to liquids' incompressible nature.

For a binary system of methane + iso-pentane, the methane richer mixtures had melting temperatures less than 100 K (98.5 K), which the optimised freeze-out model represented the experimental points accurately. However, the iso-pentane richer mixture with melting temperatures of 105.4 K had higher deviations from the predicted values. The overall deviation observed in methane + iso-pentane binaries had RMS values of (1 and 0.8) K for the default and optimised freeze-out models, respectively.

6. Acknowledgment

This research was funded by Woodside Energy Limited with further scholarship support for Mr Mirhadi Seyyed Sadaghiani through Australian Government International Research Training Program (RTP) and University Western Australia Ad-Hoc Scholarships.

7. Reference

- [1] Kumar S, Kwon H-T, Choi K-H, Lim W, Cho JH, Tak K, et al. LNG: An eco-friendly cryogenic fuel for sustainable development. *Appl Energy* 2011;88:4264–73. doi:<https://doi.org/10.1016/j.apenergy.2011.06.035>.
- [2] BP Statistical Review of World Energy 2019.
- [3] Pospíšil J, Charvát P, Arsenyeva O, Klimeš L, Špiláček M, Klemeš JJ. Energy demand of liquefaction and regasification of natural gas and the potential of LNG for operative thermal energy storage. *Renew Sustain Energy Rev* 2019;99:1–15. doi:<https://doi.org/10.1016/j.rser.2018.09.027>.
- [4] Hisazumi Y, Yamasaki Y, Sugiyama S. Proposal for a high efficiency LNG power-

- generation system utilizing waste heat from the combined cycle1Published in co-operation with the Japanese Society of Energy Resources.1. Appl Energy 1998;60:169–82. doi:[https://doi.org/10.1016/S0306-2619\(98\)00034-8](https://doi.org/10.1016/S0306-2619(98)00034-8).
- [5] Baccanelli M, Langé S, Rocco M V, Pellegrini LA, Colombo E. Low temperature techniques for natural gas purification and LNG production: An energy and exergy analysis. Appl Energy 2016;180:546–59. doi:<https://doi.org/10.1016/j.apenergy.2016.07.119>.
- [6] Siahvashi A, Al Ghafri SZS, Yang X, Rowland D, May EF. Avoiding costly LNG plant freeze-out-induced shutdowns: Measurement and modelling for neopentane solubility at LNG conditions. Energy 2021;217:119331. doi:[10.1016/j.energy.2020.119331](https://doi.org/10.1016/j.energy.2020.119331).
- [7] Sampson CC, Metaxas PJ, Siahvashi A, Stanwix PL, Graham BF, Johns ML, et al. Measurements of solidification kinetics for benzene in methane at high pressures and cryogenic temperatures. Chem Eng J 2020:127086. doi:<https://doi.org/10.1016/j.cej.2020.127086>.
- [8] Siahvashi A, Al Ghafri SZ, May EF. Solid-fluid equilibrium measurements of benzene in methane and implications for freeze-out at LNG conditions. Fluid Phase Equilib 2020;519:112609. doi:[10.1016/j.fluid.2020.112609](https://doi.org/10.1016/j.fluid.2020.112609).
- [9] Sampson CC, Metaxas PJ, Siahvashi A, Stanwix PL, Graham BF, Johns ML, et al. Measurements of solidification kinetics for benzene in methane at high pressures and cryogenic temperatures. Chem Eng J 2021;407:127086. doi:[10.1016/j.cej.2020.127086](https://doi.org/10.1016/j.cej.2020.127086).
- [10] Baker C, Siahvashi A, Oakley J, Hughes T, Rowland D, Huang S, et al. Advanced predictions of solidification in cryogenic natural gas and LNG processing. J Chem Thermodyn 2019;137:22–33. doi:[10.1016/J.JCT.2019.05.006](https://doi.org/10.1016/J.JCT.2019.05.006).

- [11] Khan MS, Lee S, Rangaiah GP, Lee M. Knowledge based decision making method for the selection of mixed refrigerant systems for energy efficient LNG processes. *Appl Energy* 2013;111:1018–31. doi:<https://doi.org/10.1016/j.apenergy.2013.06.010>.
- [12] Qyyum MA, Duong PLT, Minh LQ, Lee S, Lee M. Dual mixed refrigerant LNG process: Uncertainty quantification and dimensional reduction sensitivity analysis. *Appl Energy* 2019;250:1446–56. doi:<https://doi.org/10.1016/j.apenergy.2019.05.004>.
- [13] He T, Lin W. Design and optimization of integrated single mixed refrigerant processes for coproduction of LNG and high-purity ethane. *Int J Refrig* 2020;119:216–26. doi:<https://doi.org/10.1016/j.ijrefrig.2020.06.033>.
- [14] Xu X, Liu J, Jiang C, Cao L. The correlation between mixed refrigerant composition and ambient conditions in the PRICO LNG process. *Appl Energy* 2013;102:1127–36. doi:<https://doi.org/10.1016/j.apenergy.2012.06.031>.
- [15] Pham TN, Long NVD, Lee S, Lee M. Enhancement of single mixed refrigerant natural gas liquefaction process through process knowledge inspired optimization and modification. *Appl Therm Eng* 2017;110:1230–9. doi:<https://doi.org/10.1016/j.applthermaleng.2016.09.043>.
- [16] Krishnamurthy G, Roberts MJ, Ott CM. Precooling strategies for efficient natural gas liquefaction. *Gas Process* 2017;September/:19–29.
- [17] Qyyum MA, He T, Qadeer K, Mao N, Lee S, Lee M. Dual-effect single-mixed refrigeration cycle: An innovative alternative process for energy-efficient and cost-effective natural gas liquefaction. *Appl Energy* 2020;268:115022. doi:<https://doi.org/10.1016/j.apenergy.2020.115022>.
- [18] Acree WE. Thermodynamic properties of organic compounds: enthalpy of fusion and

- melting point temperature compilation. *Thermochim Acta* 1991;189:37–56.
doi:10.1016/0040-6031(91)87098-H.
- [19] Preston GT, Funk EW, Prausnitz JM. Solubilities of hydrocarbons and carbon dioxide in liquid methane and in liquid argon. *J Phys Chem* 1971;75:2345–52.
doi:10.1021/j100684a020.
- [20] Parks GS, Huffman HM. Some Fusion and Transition Data for Hydrocarbons. *Ind Eng Chem* 1931;23:1138–9. doi:10.1021/ie50262a018.
- [21] Schumann SC, Aston JG, Sagenkahn M. The Heat Capacity and Entropy, Heats of Fusion and Vaporization and the Vapor Pressures of Isopentane. *J Am Chem Soc* 1942;64:1039–43. doi:10.1021/ja01257a007.
- [22] Arora A. *Hydrocarbons (Alkanes, Alkenes And Alkynes)*. Discovery Publishing House; 2006.
- [23] Joint Committee For Guides In. Evaluation of measurement data — Guide to the expression of uncertainty in measurement. *Int Organ Stand Geneva* ISBN 2008;50:134.
doi:10.1373/clinchem.2003.030528.
- [24] Siahvashi A, Al-Ghafri SZS, Oakley JH, Hughes TJ, Graham BF, May EF. Visual Measurements of Solid-Liquid Equilibria and Induction Times for Cyclohexane + Octadecane Mixtures at Pressures to 5 MPa. *J Chem Eng Data* 2017;62:2896–910.
doi:10.1021/acs.jced.7b00171.
- [25] Siahvashi A, Al Ghafri SZ, Hughes TJ, Graham BF, Huang SH, May EF. Solubility of p-xylene in methane and ethane and implications for freeze-out at LNG conditions. *Exp Therm Fluid Sci* 2019;105:47–57. doi:10.1016/J.EXPTHERMFLUSCI.2019.03.010.
- [26] Lemmon, E. W.; Bell, I. H.; Huber, M. L.; McLinden, M. O. NIST Standard Reference

- Database 23: Reference Fluid Thermodynamic and Transport Properties-REFPROP, Version 10.0; National Institute of Standards and Technology, 2018; <https://www.nist.gov/srd/ref.n.d>.
- [27] Baker C, Siahvashi A, Oakley J, Hughes T, Rowland D, Huang S, et al. Advanced predictions of solidification in cryogenic natural gas and LNG processing. *J Chem Thermodyn* 2019;137:22–33. doi:10.1016/J.JCT.2019.05.006.
- [28] Baker CJ, Oakley JH, Rowland D, Hughes TJ, Aman ZM, May EF. Rapid Simulation of Solid Deposition in Cryogenic Heat Exchangers to Improve Risk Management in Liquefied Natural Gas Production. *Energy and Fuels* 2018;32:255–67. doi:10.1021/acs.energyfuels.7b03057.
- [29] Prausnitz JM, Lichtenthaler RN, Azevedo EG. *Molecular thermodynamics of fluid-phase equilibria*. Upper Saddle River, N.J.: Prentice Hall PTR.; 1999.
- [30] Yaws CL, Lin S-C. Chapter 11 - Enthalpy of fusion at freezing point—Organic compounds. In: Yaws CLBT-TP of C and H, editor., Norwich, NY: William Andrew Publishing; 2009, p. 552–91. doi:<https://doi.org/10.1016/B978-081551596-8.50016-X>.
- [31] Goodman BT, Wilding WV, Oscarson JL, Rowley RL. A note on the relationship between organic solid density and liquid density at the triple point. *J Chem Eng Data* 2004;49:1512–4. doi:10.1021/je034220e.
- [32] Matsumoto T, Miyamoto H. PpT and saturation properties of isopentane at T=(280–440)K and up to 200MPa. *J Chem Thermodyn* 2016;101:150–6. doi:<https://doi.org/10.1016/j.jct.2016.05.019>.
- [33] Lasdon LS, Waren AD, Jain A, Ratner M. Design and Testing of a Generalized Reduced Gradient Code for Nonlinear Programming. *ACM Trans Math Softw* 1978;4:34–50.

doi:10.1145/355769.355773.

- [34] Prodany NW, Williams B. Vapor-Liquid Equilibria in Methane-Hydrocarbon Systems. *J Chem Eng Data* 1971;16:1–6. doi:10.1021/je60048a015.
- [35] Lemmon EW, Span R. Short fundamental equations of state for 20 industrial fluids. vol. 51. 2006. doi:10.1021/je050186n.
- [36] Würflinger A, Kreutzenbeck J. Differential thermal analysis at high pressures- VIII: Phase behaviour of solid cyclopentanone, cyclopentanol, and cyclohexanone up to 3 KBAR. *J Phys Chem Solids* 1978;39:193–6. doi:10.1016/0022-3697(78)90042-2.
- [37] He T, Mao N, Liu Z, Qyyum MA, Lee M, Pravez AM. Impact of mixed refrigerant selection on energy and exergy performance of natural gas liquefaction processes. *Energy* 2020;199:117378. doi:10.1016/j.energy.2020.117378.